Fire Safety Journal 91 (2017) 872–881

Contents lists available at ScienceDirect

Fire Safety Journal

journal homepage: www.elsevier.com/locate/firesaf

IAFSS 12th Symposium 2017

Real-time wildland fire spread modeling using tabulated flame properties

Matthieu de Gennaro[a,b], Yann Billaud[c], Yannick Pizzo[b], Savitri Garivait[d], Jean-Claude Loraud[b], Mahmoud El Hajj[a], Bernard Porterie[b,*]

[a] NOVELTIS, 153 rue du Lac, Labège, France
[b] Aix Marseille Université, CNRS, IUSTI UMR 7343, Marseille, France
[c] Institut Pprime, CNRS-Université de Poitiers-ENSMA, Poitiers, France
[d] King Mongkut's University of Technology Thonburi, JGSEE, Bangkok, Thailand

ARTICLE INFO

Keywords:
Wildfires
Tabulation
Genetic algorithm
Real-time simulation
Front-tracking method

ABSTRACT

This paper is an extension of previous papers [1,2] on a raster-based fire spread model which combines a network model to represent vegetation distribution on land and a physical model of the heat transfer from burning to unburnt vegetation items, and takes into account local conditions of wind, topography, and vegetation. The physical model, still based on the unsteady energy conservation in every fuel element and detailed local and non-local heat transfer mechanisms (radiation from the flaming zone and embers, surface convection, and radiative cooling from the heated fuel element to the environment), now includes wind-driven convection through the fuel bed. To address the challenge of real-time fire spread simulations, the model is also extended in two ways. First, the Monte Carlo method is used in conjunction with a genetic algorithm to create a database of radiation view factors from the flame to the fuel surface for a wide variety of flame properties and environment conditions. Second, the front-tracking method, drafted in [2], is extended to polydisperse networks and implemented in the new version of the model, called SWIFFT. Finally, the SWIFFT model is validated against data from different fire scenarios, showing it is capable of capturing the trends observed in experiments in terms of rate of spread, and area and shape of the burn, with reduced computational resources.

1. Introduction

Currently there are two major approaches to model fire spread: the raster-based approach and the vector-based approach [3]. In the raster-based approach fire spread is treated as a series of cell-to-cell interactions, a set of rules defining the spread mechanism from a cell to its neighbors (see for example [4–9]). The vector-based approach assumes the propagation of the fire front as a continuously expanding polygon and is the basis of the most widely used fire spread models: FARSITE [10], PROMETHEUS [11], and SiroFire [12]. The strengths and weaknesses of both approaches are extensively discussed in [3,13]. One of the main advantages of the raster-based approach is that it is computationally less intensive and is much more suited to heterogeneous fuel and weather conditions [3]. These features led us to develop a fire spread model based on raster implementation [1,2]. The model combined a monodisperse network (i.e. one in which the fuel elements are close to a single size) to represent vegetation distribution on land with an unsteady physical model of the heat transfer from burning to unburnt fuel elements. The preheating energy-transfer mechanisms considered were: radiation from the flaming zone and embers; surface convection; and radiative cooling from the heated fuel element to the environment. At each time step, overhead flame radiation was calculated by coupling the solid flame model with the Monte Carlo method.

In the continuation of these studies, we present here the enhancements of the fire spread model that are now being included to improve the scope and validity of the model, and to reduce the computational resources needed to perform simulations. First, in order to improve model predictions of wind-driven fires through highly porous fuels, wind-driven convection inside the fuel bed is included in the model. The second enhancement concerns the calculation of flame radiation during fire spread. Although it provides high accuracy, this calculation requires a large amount of computational resources, which is incompatible with the operational needs of fire and land management services. In order to run real-time fire spread simulations, radiation calculation is thus performed using a precomputed database of view factors (VF) from the flame to the fuel surface for a wide variety of flame properties and environment conditions. Finally, the front-tracking method, used to track the fire-front interface by a moving separate grid of lower dimension than the fixed DEM grid [2], is extended to

* Corresponding author.
E-mail address: bernard.porterie@univ-amu.fr (B. Porterie).

http://dx.doi.org/10.1016/j.firesaf.2017.03.006
Received 24 February 2017; Accepted 15 March 2017
Available online 10 April 2017
0379-7112/

Nomenclature

a	fuel bed absorptivity
a,b,c	ellipse parameters (or genes) (m)
c_p	specific heat (J/kg/K)
d_{ij}	distance between cells i and j (m)
D	diameter (m)
E	emissive power (W/m²)
F	view factor
h	heat transfer coefficient (W/m^2/K)
H	height (m)
k	thermal conductivity (W/m/K)
L	length (m)
L_{vap}	latent heat of vaporization (J/kg)
m	mass
m''	mass per unit area (kg/m^2)
$\vec{n}$	unit normal vector
N	number of radiation quanta
N_{bc}	number of burning cells
Pr	Prandtl number
q	volumetric energy flux (W/m^3)
$\dot{Q}$	heat release rate (W)
S	surface area (m^2)
t	time (s)
T	temperature (K)
U	velocity (m/s)
V	volume (m^3)

Greek

α	volume fraction of fine fuel elements
δ	mean free path of radiation (m)
ε	emissivity
θ	flame angle (rd)
ν	kinematic viscosity (m^2/s)
ρ	density (kg/m^3)
σ	Stefan-Boltzmann constant (W/m^2/K^4) surface to volume ratio (m^{-1})
τ	flame residence time (s)
χ^r	radiant fraction of the heat release lost by the flame

Subscripts

i	burning cell
ij	from cell i to cell j
j	unburnt receptive cell
0	initial
∞	environment

Superscripts

c	convection
e	embers
f	flame
i	internal
ign	ignition
l	lost by radiation
m	radiation view factor
r	radiation
s	surface
$''$	per unit fuel element area
w	water

Acronyms

DFF	Dry Fine Fuel elements
DEM	Digital Elevation Model
FT	Front Tracking
MCM	Monte Carlo Method
noFT	no Front Tracking
RD	Radiation Database
VF	View Factor
WFF	Wet Fine Fuel elements

polydisperse networks (i.e. composed of fuel elements of different sizes) and implemented in the new version of the model, called SWIFFT.

2. Model overview

2.1. Governing equations and assumptions

Vegetation is here depicted as a monodisperse or polydisperse network of combustible fuel elements, or cells, that can be distributed on the soil surface either randomly or regularly depending on the coverage and spatial arrangement of vegetation, leading to either an amorphous or a crystalline network. As shown in Fig. 1, a receptive cell j may be exposed to overhead flame radiation q_{ij}^{rf}, ember radiation q_{ij}^{re}, surface and internal convection, q_{ij}^{cs} and q_{ij}^{ci}, from the burning cells ($i = 1$ to N_{bc}), while it may loss heat by radiation to the environment, q_j^{rl}. The fire spread model is based on the energy conservation equation assuming that:

H1. Each combustible cell j(e.g. a tree or a shrub) has a cylindrical shape with a height H_j and a diameter D_j. The elementary volume involved in preheating is a top layer of the fuel element with a thickness δ_j and a volume $V_j=\pi D_j^2\delta_j/4$. The thickness δ_j, which cannot exceed H_j, corresponds to the mean free path of radiation through the cell. It can be related to the surface-to-volume ratio of fine fuel elements, σ_j, and to the volume fraction of fine fuel elements, α_j, as $\delta_j=min(4/\sigma_j\alpha_j; H_j)$ [14,15]. This implies that for a travel distance greater than δ_j the medium does not interact with radiation.

H2. Wildfire spread is dominated by the fine, thermally-thin vegetative fuels (grass and foliage of shrubs and trees), while the thicker fuel elements, typically greater than 6 mm in diameter burn more slowly at the back of the fire front [16,17] and do not contribute to fire spread.

H3. As is commonly the case in fire models involving fine wildland fuels, the thermally thin assumption is adopted here, which means that there is no temperature difference in the control volume. This is assumed to apply if δ_j is small compared to flame length.

H4. The thermal response of wet fine fuel (WFF) matter to heating involves three successive paths [18]. First, wet fine fuel elements rise in

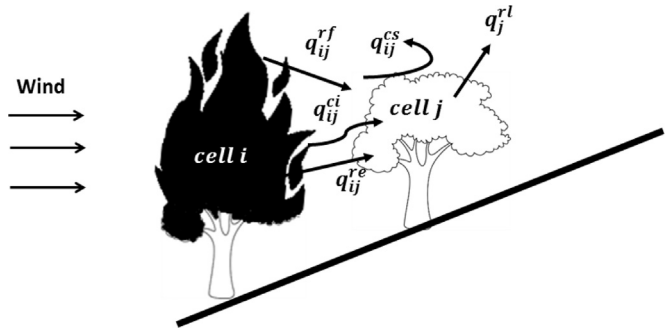

Fig. 1. Flame spread schematic, with energy-transfer mechanisms indicated.

temperature, up to 373 K (evaporation at less than the boiling temperature of water is assumed to be negligible); second, phase change of water to vapor occurs at 373 K, until all the moisture has evaporated; and third, the dry fine fuel (DFF) elements thus formed rise in temperature, up to the ignition temperature. Flammable vapors are generated and burn in the gas phase. Once all the pyrolyzates are depleted in the particle, flaming ceases. If oxygen is present, glowing combustion of the char occurs. In the present work, the contribution of char combustion to fire spread is ignored.

H5. The emissivity of embers is equal to one and their temperature to the flame temperature [18], which leads to the emissive power of the embers $E_j^e = \sigma T_j^{f\,4}$.

H6. Since char combustion is ignored, the volume of the solid phase, and thus its volume fraction, α_j, remains constant throughout the degradation process. It can be deduced from the density and mass of DFF per unit cell area as: $\alpha_j = m_j^{DFF''}/\rho_j^{DFF} H_j$.

H7. Other energy-transfer mechanisms of preheating, such as turbulent diffusion, solid- and gas-phase conduction and convective cooling, as well as the energy absorbed by pyrolysis prior to ignition, are negligible [19].

Based on the previous assumptions, the energy conservation equation applied to the control volume V_j of a receptive cell j exposed to N_{bc} burning cells can be written, depending on the degradation path considered, as follows.

Heating of WFF ($T_j < 373K$ and $m_j^{w''} = m_{0j}^{w''}$):

$$\alpha_j \rho_j^{WFF} \frac{d\left(c_{p_j}^{WFF} T_j\right)}{dt} = S_q \tag{1}$$

Drying of WFF ($T_j = 373K$):

$$-\frac{L_{vap}}{H_j}\frac{dm_j^{w''}}{dt} = S_q \tag{2}$$

Heating of DFF ($373K < T_j < T_j^{ign}$ and $m_j^{w''} = 0$):

$$\alpha_j \rho_j^{DFF} \frac{d\left(c_{p_j}^{DFF} T_j\right)}{dt} = S_q \tag{3}$$

where $S_q = \sum_{i=1}^{N_{bc}} (q_{ij}^{rf} + q_{ij}^{re} + q_{ij}^{ci} + q_{ij}^{cs}) - q_j^{rl}$, T_j and $m_j^{w''}$ are the temperature and current mass of water per unit area of cell j. The specific heat of WFF of cell j can be calculated as

$$\rho_j^{WFF} c_{p_j}^{WFF} = \rho_j^{DFF} c_{p_j}^{DFF} + \rho_j^{DFF} \frac{m_j^{w''}}{m_j^{DFF''}} c_p^{\,w} \tag{4}$$

The specific heat of DFF, $c_{p_j}^{DFF}$, depends on temperature according to $c_{p_j}^{DFF} = 1110 + 3.7T_j$ [20], which implies that an iterative procedure must be used to calculate temperature from enthalpy. Note that the term $m_j^{w''}/m_j^{DFF''}$ represents the current fuel moisture content, determined on a dry basis.

The term q_{ij}^{cs} corresponds to the surface convection preheating of cell j by the hot gases coming from the burning cell i of the flame front. As underlined by Beer and Enting [21], the flame is not an impermeable barrier and, as a result of three-dimensional effects, the wind can penetrate the flame region. Therefore, the surface of an unburned cell j located in the wake of a burning cell i will be heated by convection as a function of the distance between them, d_{ij}, according to an exponential decay law with a characteristic length of about three times the flame length [19]

$$q_{ij}^{cs} = \frac{h^{cs}}{\delta_j}(T_i^f - T_j) exp\left(-\frac{d_{ij}}{3.33 L_i^f}\right) \tag{5}$$

where h^{cs} is an average heat transfer coefficient for turbulent flow over a flat plate [22],

$$h^{cs} = 0.037 \frac{k}{d_{ij}}\left(\frac{U_j^t d_{ij}}{\nu}\right)^{0.8} Pr^{1/3} \tag{6}$$

In Eq. (6), U_j^t is the tangential component of the local wind velocity at the top of cell j, k and ν are the thermal conductivity and kinematic viscosity of air evaluated at the average of the flame and environment temperatures.

Burning embers lose heat by radiative transfer which contributes to the preheating of neighboring unburned cells j. Using the Beer-Lambert law, internal radiation decays exponentially with the distance d_{ij} as

$$q_{ij}^{re} = \frac{1}{\delta_j} E_i^e exp(-0.25\sigma_j \alpha_j d_{ij}) \tag{7}$$

where E_i^e is the emissive power of embers (see assumption H5). As they rise in temperature, unburnt cells $j$lose heat to the environment by radiation, so that

$$q_j^{rl} = \frac{1}{\delta_j}\varepsilon_j \sigma (T_j^4 - T_\infty^4) \tag{8}$$

where ε_j is the emissivity of cell j and T_∞ the environment temperature.

A focus is given below on the main enhancements from the previous model [1,2], including wind-driven convection within the fuel bed, radiation based on tabulated flame properties and front tracking.

2.2. Wind-driven convection within the fuel bed

For highly porous fuel beds, convection through the fuel bed can contribute significantly to fire spread [19]. The internal convective preheating of cell j by the gases heated by the embers of cell i can be expressed as follows [18]

$$q_{ij}^{ci} = \sigma_j \alpha_j h^{ci} (T_i^e - T_j) exp(-0.25\sigma_j \alpha_j d_{ij}) \tag{9}$$

where

$$h^{ci} = 0.911 \frac{k}{D_j^b}\left(\frac{U_j^t D_j^b}{\nu}\right)^{0.385} Pr^{1/3} \tag{10}$$

In Eq. (10), U_j^t is the tangential component of the local wind velocity at the mid-height of cell j, $k$and ν are the thermal conductivity and kinematic viscosity of air evaluated at the ember temperature. As done previously for surface convection preheating, the ray tracing method is used to calculate the term q_{ij}^{ci}.

2.3. Overhead flame radiation

The amount of radiant energy received by the receptive cell j from the flame attached to a burning cell i depends on flame emission, as well as its attenuation by the air layer in between, and its absorption by the fuel cell j. Overhead flame radiation can be calculated by combining the Monte Carlo ray tracing method with the solid flame model [1,23], which requires estimates of flame properties: length L_i^f, base diameter D_i^f (here, $D_i^f = D_i$), tilt angle θ_i^f, and emissive power $P_i^{f'''}$. The Monte Carlo ray tracing method can be used to determine the amount of radiation quanta N_{ij}launched from the burning cell i that finally reaches the receptive cell j. Every bundle represents a certain quantity of radiative power $P_i^{f'''} S_i^f / N_i$ where N_i is the total number of bundles emitted from the flame surface area S_i^f. The radiative gain from cell i to cell j can thus be written using the view factor from the flame above the cell i to a unit area of cell j, $F_{ij} = N_{ij}/N_i$, as

$$q_{ij}^{rf} = a_j P_i^{f'''} S_i^f F_{ij}/V_j \tag{11}$$

Two different corrections on the radiative gain were applied. First, radiation can be absorbed by any cell k (or a part of it) located on the path between i and j. It can also be absorbed by the flame attached to cell k, if k is a burning cell. Second, radiation can be attenuated by the

atmospheric layer between cells i and j. The attenuation was calculated from the Beer-Lambert law, in terms of transmittance as a function of the air layer properties (thickness d_{ij} and relative humidity RH) and source temperature [1].

Applying the Monte Carlo method for every burning site at each time step during fire spread is very CPU time consuming due to the large number of bundles launched per unit flame area. A way to limit this drawback is to pre-calculate the view factors F_{ij} from the cylindrical flame attached to cell i to any unit area of the top surface of cell j for a wide variety of flame and environment conditions. The idea came from the nearly elliptical shape of the iso-view-factors calculated using the Monte Carlo calculations, as shown in Fig. 2 for a flame of diameter 2 m and height 5 m, and a tilt angle of 30° (here, $RH = 20\%$, the cylindrical flame is discretized into 120×60 equal-area diffuse black facets and the number of photon bundles emitted per unit area from the flame surface is 10^7). Therefore, in the proposed methodology, we assume that any iso-VF, F_m, can be approximated by an ellipse whose parameters, namely the semi-major axis a_m, the semi-minor axis b_m, and the distance between the center of cell i and the center of the ellipse c_m (Fig. 3a), depend on the flame properties and relative humidity (RH) of air. Literature provides various approaches to solving the ellipse fitting problem based on a given set of data points in the plane and is most often based on algebraic or least-square distance minimization methods, arc-based or fuzzy clustering techniques, or a genetic algorithm (GA) (see [24–28] to name but a few). The latter approach is used in the present study.

Genetic algorithms were developed to mimic some principles of natural selection and evolution. In the present application of GA, each set of parameters $\{a_m, b_m, c_m\}$represents one individual in a population. The first population is randomly selected from a predefined range. Each individual is tested against the experimental data F_m and the goodness of the fit is measured using a fitness function. The population undergoes a set of operations: selection, reproduction, mutation and crossover, which results in a next generation. The process is repeated generation after generation, thus improving successive generations, until convergence towards the best fitting individuals is achieved.

The proposed methodology consists of three steps: first, for a given set of flame properties and environment RH values, the Monte Carlo method is used to calculate the field of view factors from the flame to the ground level; second, for a user-defined value of the iso-VF, F_m, a genetic algorithm is used to fit an ellipse of parameters $\{a_m, b_m, c_m\}$to the set of points in the horizontal plane where the value of the view factor is sufficiently close to F_m, and this operation is repeated as many times as necessary, depending on the total number of iso-VFs, m, considered; and third, a database of radiation VF is created by varying, over a wide range, the flame properties and RH values.

An example is given in Fig. 3, where the GA is used to determine the iso-VF ellipses which correspond to the conditions of Fig. 2. The number of iso-VFs considered is set to $m = 40$ from 0.001 to 0.9, while being tightened when approaching the flame due to the non-linear behavior of radiation attenuation with distance from the flame. The agreement between the ellipses and each cluster of points A_m on the ground level where the value of the iso-VF is sufficiently close to F_m for $1 \leq m \leq 40$, within a relative tolerance of 0.001, is excellent.

2.4. The front-tracking method

The front-tracking method consists in tracking the fire front by a moving separate grid of lower dimension than the fixed DEM grid. As fire spread, fuel items are generated “on the fly” in the very few grid pixels of the DEM attached to the fire front, namely all the active DEM pixels where fuel elements are heated or burning and their nearest neighboring pixels. All the information required for fire spread is contained in these pixels. The method is based on the concept of double indexing: a global indexing of the active DEM pixels and a local indexing of the vegetation items in the active DEM pixels. The main task consists in finding the neighbors of any burning fuel item that belongs to a DEM pixel. This can be divided into two stages: first, the eight neighboring DEM pixels are identified; second, the fuel items belonging to these pixels are numbered and stored. This avoids searching into the whole domain all fuel items that could be involved in the preheating process. When all the fuel items in any active DEM pixel are burned or no longer under the influence of the flame front, the active DEM pixel is rendered inactive and its storage is deallocated. The front-tracking method, first drafted in [2], is extended to polydisperse networks and implemented in the new version of the model.

2.5. Input data and model parameters

Input data are the following:

1. Topography: a DEM which is a digital file consisting of terrain elevations for ground positions at regularly spaced horizontal intervals.
2. Vegetation map and coverage (i.e. the fraction of soil which is covered by vegetation).
3. Meteorological conditions (as provided by a weather station): average wind speed (U_∞) and direction, environment temperature (T_∞), and relative humidity of air (RH). Local wind speed and direction are calculated from average values using a numerical model based on CALMET [29] which takes into account the combined effects of the topography and surface roughness of the land site [30], at a resolution twice that of DEM.
4. A database of radiation VF for a wide range of flame properties and RH values.
5. For any vegetation cell j: height and diameter (H_j, D_j), emissivity (ε_j), surface-to-volume ratio of fine fuel elements σ_j, initial masses of DFF and water per unit area ($m_j^{DFF''}$, $m_{0j}^{w''}$), and density of DFF (ρ_j^{DFF}).
6. For each burning cell i, flame residence time (τ_i), heat of combustion of volatiles (Δh_i), ignition temperature (T_i^{ign}), and radiant fraction of the heat release rate lost by the flame (χ_i^r).

Model parameters are determined following the sequence of operations given by the flowcharts of Fig. 4. The original procedure can be found in [1]. It is here extended to a polydisperse network composed of vegetation items, which may differ in size and properties.

As a first approximation, the pyrolysis rate may be related to the mass of DFF per unit area and flame residence time as $\dot{m}_i^{DFF''} = m_i^{DFF''}/\tau_i$. Since flaming combustion corresponds to the chemical reaction of volatiles with air, the associated heat release rate may be expressed in terms of the initial loading of DFF, heat of combustion of volatiles, and cell area, $S_i = \pi D_i^2/4$, as $\dot{Q}_i = \dot{m}_i^{DFF''} \Delta h_i S_i$. As wind has little influence on flame length [31–33], the flame length, L_i^f, is assumed to be equal to the luminous flame height with no wind, that can be deduced from the heat release rate and burning cell diameter as

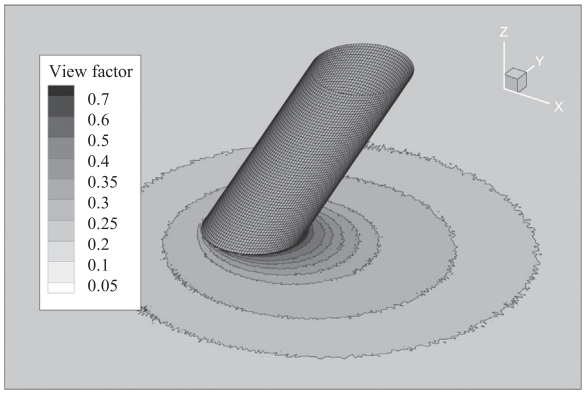

Fig. 2. Field of view factor from a tilted flame to the ground level.

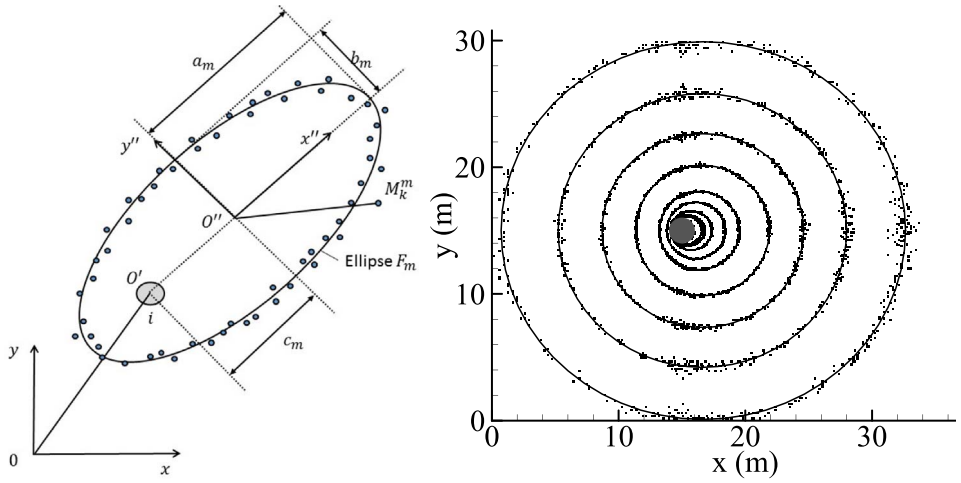

Fig. 3. Left: coordinate system attached to a burning site i. Right: selection of iso-VF ellipses determined by the GA for the conditions of Fig. 2: F = 0.37,0.31, 0.22,0.14,0.84 × 10^{-1},3.13 × 10^{-2},1.17 × 10^{-2},4.38 × 10^{-3},1.64 × 10^{-3}. The gray disk represents the base of the flame.

[34]: $\widetilde{H}_i^f$=0.0148$\dot{Q}_i^{0.4}$−1.02D_i. The luminous flame height under the influence of wind is estimated from the Putnam's correlation [35]: $H_i^f = \widetilde{H}_i^f\left(1 + 4\frac{U_i^{t2}}{g\widetilde{H}_i^f}\right)^{-0.5}$ where U_i^t is evaluated at the top of cell i. Following Albini [36], the tangent of the flame angle, defined as the angle between the flame axis and the normal to the terrain surface, is found to be proportional to the square root of the Froude number $Fr_i = U_i^{t2}/(gH_i^f)$ as: $tan\theta_i$=1.22$Fr_i^{0.5}$. The emissive power per unit area of the flame may be evaluated from the following equation: $P_i^{f''}=\chi_i^r\dot{Q}_i/(\pi D_i L_i^f)$. As a first approximation, the flame temperature may be deduced from the emissive power assuming that the flame is a gray solid body, according to: $T_{f,i}^4 = P_i^{f''}/(\varepsilon_i^f\sigma)$, where ε_i^f is the flame emissivity, which can be approximated as a function of the flame length and an effective total absorption coefficient of 0.6 m^{-1}: ε_i^f=1 − $e^{-0.6L_i^f}$ [18]. For inclined terrains, the local effects of wind and slope on flame geometry are combined in a vectorial manner.

3. Model validation

The SWIFFT model is applied to three different fire scenarios: a grassland fire experiment in Australia [37,38], a prescribed burning in Thailand (present study), and an arson Mediterranean fire that occurred in Favone in Corsica in 2009 [39]. They differ mainly in the mechanism of heat transfer responsible for fire spread. The parameters used for the simulations are summarized in Table 1.

3.1. Australian grassland fire experiment

Results from grassland experiments conducted in Australia in 1986 [37,38] provide a useful set of data for model evaluation (see for example [41–43]). In this section, SWIFFT predictions of fire perimeters from the experimental case F19 are presented. In F19, the plot was 200m × 200m and composed of *Themeda* grass (kangaroo grass). The fire was lit from a 175 m-long ignition line perpendicular to the prevailing wind on the upwind edge of the plot. This line fire was created with drip torches carried by two field workers walking for 56 s (87.5 m) in opposite directions from the center point to the ends the line fire. As observed by Cheney and co-workers, grass layers were continuous and homogeneous, which led us to use a triangular “crystalline” network, with a vegetation coverage of 0.91. The sizes of vegetation items were deduced from the correlation of Heskestad [34] using the flame heights observed experimentally [37]. The wind speeds at 2m above ground level at each corner of the experimental plot were measured at 5 s intervals throughout the duration of the fire. Measured fire perimeters are plotted at times t = 56$s$and 86s [37] in Fig. 5. They are compared with those predicted by SWIFFT using the parameter values given in Table 1.

The average rate of spread of the head fire is slightly overestimated,

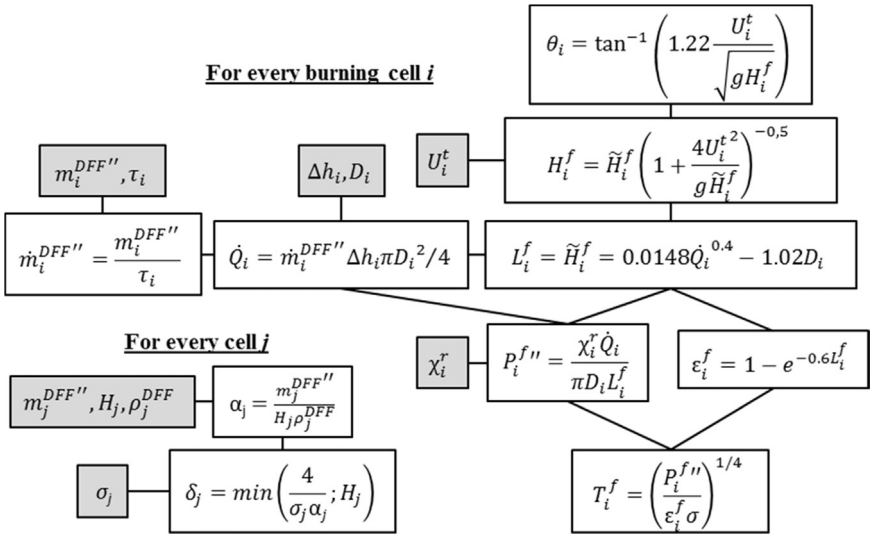

Fig. 4. Organizational charts for the calculation of model parameters.

Table 1
Input data and model parameters used for fire spread model calculations.

Input model parameters (units)	Australian grassland fire experiments [37,38]	Thai fire experiments (present study)	Mediterranean Fire [39]
Network	200 m×200 m Mono-disperse triangular	~150 m×50 m Poly-disperse amorphous using a normal size distribution (mean diameter: 0.25 m, deviation: 0.04 m)	1 km×0.5 km Mono-disperse triangular
Resolution of DEM and fuel map (m)	1	1	25
U(m/s)	4.83 (at 2 m AGL*)	0.75 (at 2.5 m AGL*)	6 (at 10 m AGL*)
T_∞ (K)	307	313	303
RH (%)	20	43	42
Δt (s)	0.2	2	1
Vegetation type	*Themeda grass* (kangaroo grass)	Mixed Deciduous Forest fuel	Mixture of live strawberry trees (*arbustus unedo*) and leaf litter
Vegetation coverage	0.91	0.7	0.91
D (m)	2.54[a]	0.25 (in average)	3
H (m)	0.51	0.04	3
$m^{DFF''}$ (kg/m²)	0.313	0.294	2.682
$m^{w''}$ (kg/m²)	0.0182	0.0168	1.582
ρ^{DFF} (kg/m³)	512	510	720
σ (1 /m)	12240	4664[b]	5154
ε	0.9	0.6[b]	0.9
τ (s)	6.2[c]	30[b]	30
Δh (MJ/kg)	14.454	13.600[b]	15.360
T^{ign} (K)	561[d]	561[d]	561[d]
χ^r	0.35[e]	0.4[e]	0.3[e]

*AGL: Above Ground Level.
[a] deduced from the observed flame height.
[b] laboratory measurement.
[c] deduced from the empirical formula from Anderson [40]: $\tau = 75600/\sigma$.
[d] as suggested by Koo et al. [18].
[e] assumed.

with an error of about 5% at $t = 5$ s (1.41 vs. 1.38 m/s) and 8% at $t = 8$ s (1.43 vs. 1.36 m/s). On the contrary, the area burned is well reproduced, with an error less than 3% at $t = 56$ s (0.80 vs. 0.82 ha) and $t = 8$ s (1.70 vs. 1.73 ha). However, behind this apparently good agreement, discrepancies between observed and predicted front shapes are observed. Changes in wind speed and direction occurred in the experiment F19 which broke the symmetry of the fire perimeter, this does not occur in the simulation since a constant wind orientation is assumed. Another excellent indicator of fire behavior is the average depth of the head fire front since this characteristic length is the product of the rate of spread and the flame residence time ($d = ros \times \tau$). SWIFFT gives approximately 9.2 m, whereas experiments gave about 10 m. It is worth noting that experimental mean values of the *ros* (calculated between 56 and 86 s) and head fire depth leads to a mean flame residence time of 7.6 s, which is slightly higher than that deduced from the Anderson formula, 6.2 s. This case requires 22 CPU seconds for 86 s of simulated time on a single 3.3-GHz Intel Xeon processor.

3.2. Thai fire experiments

A series of prescribed burning experiments was conducted as part of the present work. The experiments took place in the north of

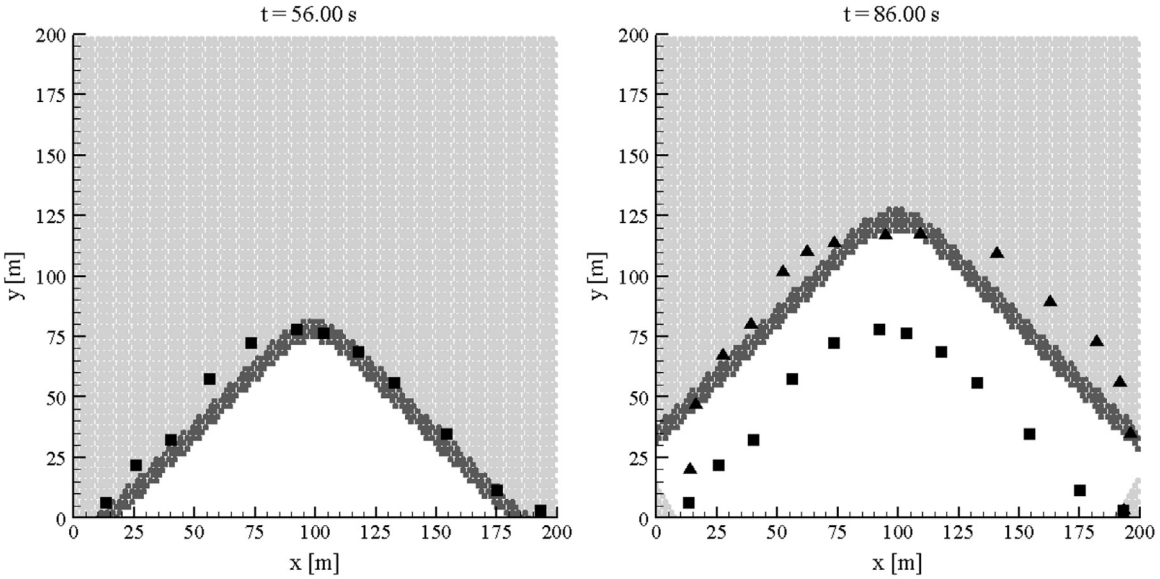

Fig. 5. Predicted and measured (symbols) fire contours at times t=5 s and 86 s for the Australian grassland fire experiment F19.

Thailand, in the province of Chiang Mai. This province is repeatedly faced with forest fires during the dry season, from December to April, and with the formation of haze associated with them. The study area is a good example of mixed deciduous forest (MDF). MDF fires are surface fires in which the fuel bed is a litter composed of biomass, including leaf litter, twigs, seedlings, and understory. Fuel loading and wind speed are generally low, which explains why MDF fires propagate slowly with relatively small flame. Thermo-physical and geometrical fuel properties were preliminarily determined in the laboratory from samples collected in the field [44] (Table 1). A 1 m-resolution DEM was built from GPS-data recordings (Trimble pro XT GPS). During the fire, meteorological data, including air temperature, relative humidity, wind speed and wind direction, were recorded at 1-min intervals. Wind data showed nearly constant direction (117°) and speed (0.75 m/s at 2.5 m above the ground level). Experimental contours were determined by recording the passage time of fire at different markers. These georeferenced markers were set regularly at 5 m intervals along 5 lines (lines A to E in Fig. 6). Thanks to a dozen rangers equipped with torches, line ignition was instantaneous and occurred on the right-hand side of the area (broken line A_0E_0 in Fig. 6). Vegetation was slightly patchy, with a vegetation coverage of approximately 0.7. It is represented as a polydisperse amorphous network, with a normal distribution of mean diameter of 0.25 m and standard deviation of 0.04 m.

In Fig. 6, SWIFFT predictions are compared with experiments. Unlike model results, experimental contours at $t =$ 20 and 40 min

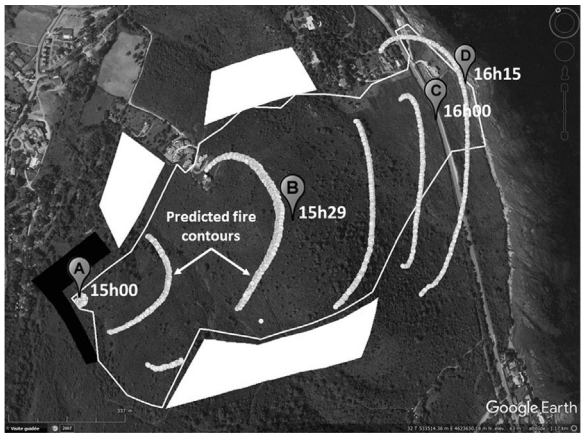

Fig. 7. predicted 15-min interval contours and post-fire GPS recordings (white line). Near the ignition point A, vegetation has been cleared (black zone). White zones correspond to the drop zones of water-bombing aircrafts. Times of fire front passage at points B to D are indicated.

(Fig. 6a and b) exhibit an S-shape. At $t =$ 40 min (Fig. 6c), fire spread is well predicted by the model along the C and D columns, but it is overestimated along the other columns. From $t =$ 60 min (Fig. 6d) both observed and predicted fire contours have a C-shape. However,

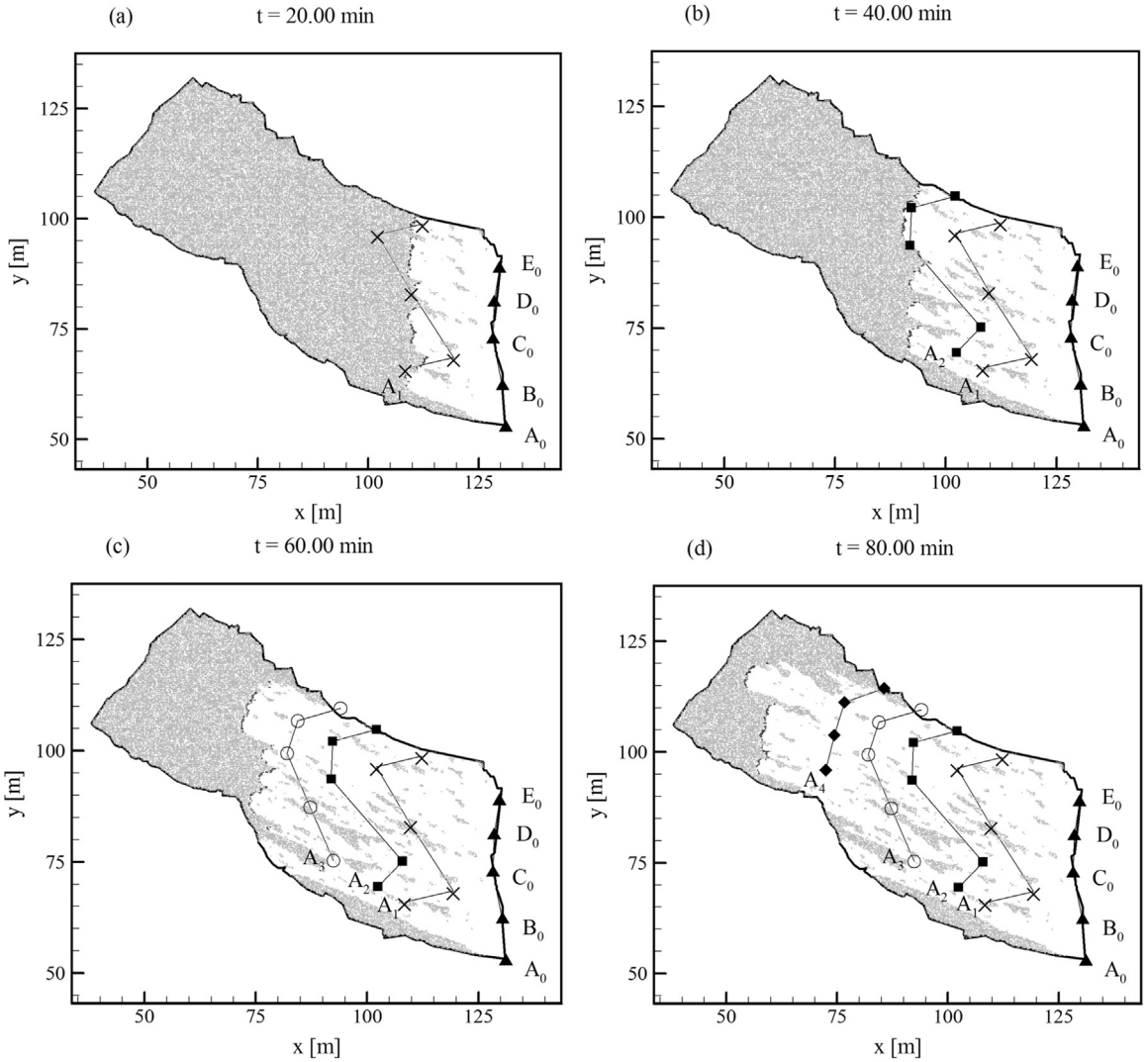

Fig. 6. Comparison between predicted and measured fire contours (black lines with symbols) at t=0 min (▲), t=20 min (×), t=40 min (■), t=60 min (○), and t=80 min (♦).

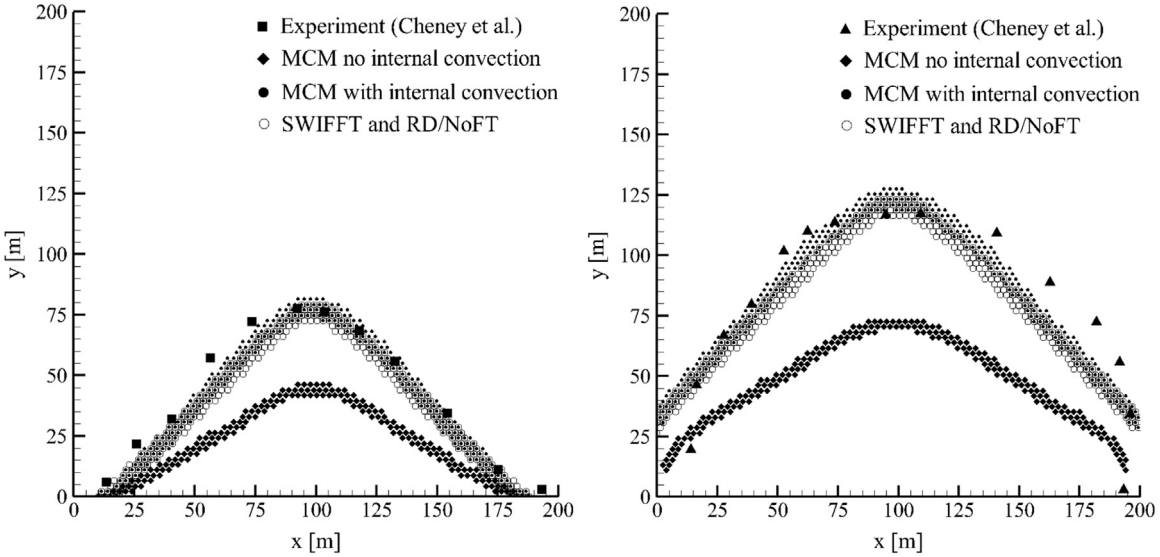

Fig. 8. Comparison between predicted and measured fire contours at times t=5 s and 86 s for the Australian grassland fire experiment F19.

Table 2
Comparison between model results and data from the Australian grassland fire experiment F19.

	Rate of spread (m/s) after 56/86 s of fire	Burned area (ha) after 56/86 s of fire	CPU time (s)[a] for 86 s of simulated time	Memory allocation (MB)
Exp.	1.38/1.36	0.82/1.73		
MCM, no internal convection	0.83/0.84	0.47/1.00	6711	171
MCM, with internal convection	1.45/1.48	0.83/1.78	18412	171
RD/noFT	1.41/1.43	0.80/1.70	94	66
SWIFFT	1.41/1.43	0.80/1.70	22	12

[a] On a single 3.3-GHz Intel Xeon processor.

the rate of spread is overestimated. This can be due to local variations in fuel distribution, as observed in the field. A better agreement should be achieved using a more detailed description of the horizontal and vertical fuel arrangement. The sensitivity of the fire spread process to fuel distribution is enhanced here by the short-range heat transfer mechanism between burning and unburned vegetation cells. As said above, MDF fires generate small and nearly vertical flames, which explains why radiation is the dominant mechanism of heating and only affects the nearest neighbors of burning cells. In this configuration, the contribution of radiation from embers is just as important as that arising from the flame. The predicted post-fire burned area is shown in Fig. 6, revealing unburned islands with an elongated shape in the main fire propagation direction, which is in qualitative agreement with field observations. This case requires 35 CPU seconds on a single 3.3-GHz Intel Xeon processor for 4800 s of simulated time.

3.3. Corsican fire

This fire has been extensively studied and documented by Santoni et al. [39]. Geographical data include a DEM and vegetation map at a resolution of 25 m. This case is of interest because the fire propagated first upslope, between points A and B (Fig. 7), downslope between points B and C, and then on a flat terrain between points C and D. The dominant vegetation was composed of a mixture of foliage of live strawberry trees (*Arbutus unedo*) and leaf litter. The weather conditions at the time of the fire were: an average wind speed of 6 m s^{-1} at 10 m above ground level, an average direction of 270° (west), and a dry bulb temperature of 303 K. Since the landscape was almost continuously covered with homogeneous vegetation, a triangular "crystalline" network is used, with a maximum vegetation coverage of 0.91. The impact of fire suppression actions is modeled by rendering inactive (fire-resistant) the vegetation items located in the drop zones of aerial water bombers (see the white zones in Fig. 7).

Comparison between predicted and real fire contours shows that the location of the head fire is fairly well predicted by SWIFFT (Fig. 7). After 29 min of upslope fire propagation (point B in Fig. 7), the average rate of spread of the head fire, calculated as the distance between points A and B divided by the time the fire front takes to travel that distance, is slightly underestimated, 16.3 vs. 17.9 m min^{-1}. The same trend is observed in the downslope part of the terrain, between points B and C, with 14.4 vs. 14.8 m min^{-1}. On the contrary, the average rate of spread between points C and D is slightly overestimated, with 11.9 vs. 9.3 m min^{-1}. Possible errors in the estimation of some input parameters and changes in wind speed and orientation, which are not taken into account in the simulation, may explain these discrepancies. Model overestimation of the lateral expansion of the fire is also visible in Fig. 7, especially after point B. As suggested by Mell et al. [42], a possibility is that the flank fires are under resolved, since their depth can be significantly smaller than head fires. This can also be attributable to the rough estimate of drop zone area and positioning. This case requires 44 CPU seconds for 4500 s of simulated time.

3.4. Model evaluation and performance

In order to measure how each enhancement influences predictive capability and computational efficiency, we evaluate models that exclude some of the enhancements. In reporting our results, we refer to the models that use the Monte Carlo method during fire spread on the fixed DEM grid with the term MCM, including or not internal convection preheating, and we refer to the model that uses the precomputed radiation database on the fixed DEM grid and internal convection preheating with the term RD/noFT. The SWIFFT model

includes all enhancements previously detailed. For a proper model comparison, the number of radiation quanta emitted per unit flame surface area is of 500 for all models. The comparison between predicted and measured fire contours for the Australian grassland fire experiment F19 [37,38] is shown in Fig. 8.

First of all, strong differences are observed between MCM results with and without internal convection. The porosity of the grassland fuel bed (0.998) is so high that the contribution of interior convection to fuel preheating is of major importance [19]. It is also found that the SWIFFT model gives strictly identical results to those without front tracking (RD/noFT), with a reduction in CPU time and memory allocation by a factor of 4.3 (22 vs. 94 s) and 5.5 (12 vs. 66 MB) (Table 2). More significantly, Fig. 8 shows that SWIFFT produces results comparable to those obtained from the variant using MCM with internal convection, with discrepancies on the average rate of spread and burned area less than 3.5% and 4.5% respectively. This relatively good agreement is accompanied by a drastic reduction in CPU time and memory allocation (Table 2), which shows the effectiveness of the enhancements made.

4. Conclusion

An improved version of a network model for simulating fire spread through vegetative fuels is presented and evaluated using observational data from different fires. In this model, called SWIFFT, the combustion process is driven by unsteady energy conservation within the fuel stratum and detailed heat transfer mechanisms: radiation from the flaming zone and embers, surface and internal convection, and radiation loss. The local effects of wind, topography, and vegetation are included. Real-time fire spread simulations are achieved by coupling a precomputed database of radiation view factor and a front-tracking method. It is found that SWIFFT is capable of capturing the trends observed in experiments in terms of the rate of spread, and the area and shape of the burn, with reduced computational resources. Differences between predictions and data are observed that can be attributable to possible errors in the estimation of model parameters and spatial heterogeneity in the fuel load distribution. It is also found that the location of the head fire is fairly well predicted, whereas SWIFFT over predicts the spread rate of fire on the flanks. Areas for future model development and evaluation include: 1) to perform a sensitivity analysis in order to evaluate the impact of parameter variations on fire propagation and thus to identify the most influential parameters; 2) to increase the raster resolution of flank fires; and 3) to extend the validation effort to a larger set of experiments and to a wider range of fuel parameters in order to better assess SWIFFT capabilities. Another way to improve the wildfire spread predictions would be to combine observational data with SWIFFT predictions through data assimilation [45].

Acknowledgments

This research was partially supported by the Commission for Higher Education in Thailand, the Thailand Research Fund, the National Science and Technology Development Agency in Thailand, the French Ministry of Foreign and European Affairs, and the French Ministry of Education and Research as part of the Hubert Curien Partnerships SIAM 2012 (No. 27571PF). MDG gratefully acknowledges the financial support from NOVELTIS and ANRT (CIFRE/ANRT contract No. 566/2013).

References

[1] Y. Billaud, N. Zekri, M. Drissi, Y. Pizzo, Z. Acem, A. Collin, P.A. Santoni, B. Bosseur, P. Boulet, B. Porterie, A hybrid small-world network/semi-physical model for Predicting wildfire spread in heterogeneous landscapes, J. Phys.: Conf. Ser. 395 (2012) 012008. http://dx.doi.org/10.1088/1742-6596/395/1/012008.

[2] Y. Billaud, M. De Gennaro, A. Kaiss, Y. Pizzo, N. Zekri, B. Porterie, Coupling a meshless front-tracking method with a hybrid model of wildfire spread across heterogeneous landscapes, in: D.X. Viegas (Ed.)Advances in Forest Fire Research, Imprensa da Universidade de Coimbra, Coimbra, 2014, p. 709/715. http://dx.doi.org/10.14195/978-989-26-0884-6.

[3] A.L. Sullivan, Wildland surface fire spread modelling, 1990–2007. 3: simulation and mathematical analogue models, Int. Wildland Fire 18 (2009) 387–403. http://dx.doi.org/10.1071/WF06144.

[4] P. Kourtz, W. O'Regan, A model for a small forest fire ... to simulate burned and burning areas for use in a detection model, For. Sci. 17 (1) (1971) 163–169.

[5] D. Green, A. Tridgell, A. Gill, Interactive simulation of bushfires in heterogeneous fuels, Math. Comput. Model. 13 (12) (1990) 57–66. http://dx.doi.org/10.1016/0895-7177(90)90099-9.

[6] M. Vasconcelos, D. Guertin, FIREMAP - simulation of fire growth with a geographic information system, Int. J. Wildland Fire 2 (2) (1992) 87–96. http://dx.doi.org/10.1071/WF9920087.

[7] W.W. Hargrove, R.H. Gardner, M.G. Turner, W.H. Romme, D.G. Despain, Simulating fire patterns in heterogeneous landscapes, Ecol. Model. 135 (2000) 243–263. http://dx.doi.org/10.1016/S0304-3800(00)00368-9.

[8] S. Berjak, J. Hearne, An improved cellular automaton model for simulating fire in a spatially heterogeneous savanna system, Ecol. Model. 148 (2) (2002) 133–151. http://dx.doi.org/10.1016/S0304-3800(01)00423-9.

[9] S. Yassemi, S. Dragićević, M. Schmidt, Design and implementation of an integrated GIS-based cellular automata model to characterize forest fire behaviour, Ecol. Model. 210 (2008) 71–84. http://dx.doi.org/10.1016/j.ecolmodel.2007.07.020.

[10] M.A. Finney, FARSITE: Fire Area Simulator-model development and evaluation. Res. Pap. RMRS-RP-4. Fort Collins, CO: U.S. Department of Agriculture, Forest Service, Rocky Mountain Research Station. 47 p, 1998.

[11] Prometheus, The Canadian Wildland Fire Growth Model (CWFGM), Prometheus ver. 5.1.8. ⟨http://www.firegrowthmodel.com/index.cfm⟩. (25 July 2008).

[12] J.R. Coleman, A.L. Sullivan, A real-time computer application for the prediction of fire spread across the Australian landscape, Simulation 67 (1996) 230–240. http://dx.doi.org/10.1177/003754979606700402.

[13] S.H. Peterson, M.E. Morais, J.M. Calson, P.E. Dennison, D.A. Roberts, M.A. Moritz, D.R. Weise, Using HFIRE for spatial modeling of fire in shrublands. Technical Report PSW-RP-259, USDA, Albany, CA, 2009.

[14] N.J. De Mestre, E.A. Catchpole, D.H. Anderson, R.C. Rothermel, Uniform propagation of a planar fire front without wind, Combust. Sci. Technol. 65 (1989) 231–244. http://dx.doi.org/10.1080/00102208908924051.

[15] B.W. Butler, Experimental measurements of radiant heat fluxes from simulated wildfire flames, – Proceedings of the 12th Conference of Fire and Forest Meteorology, pp. 104–111, 1993.

[16] R.H. Luke, A.G. McArthur, Bushfires in Australia, Australian Government Publishing Service, Canberra, 1977.

[17] J.D. Cohen, M.A. Finney, Fine fuel particle heating during experimental laboratory fires, in: D.X. Viegas (Ed.)Advances in Forest Fire Research, Imprensa da Universidade de Coimbra, Coimbra, 2014. http://dx.doi.org/10.14195/978-989-26-0884-6_24.

[18] E. Koo, P.J. Pagni, J. Woycheese, S. Stephens, D.R. Weise, J. Huff, A simple physical model for fire spread rate, – in: Proceedings of the Eighth International Symposium, International Association for Fire Safety Science, pp. 851–862. http://dx.doi.org/10.3801/IAFSS.FSS.8-851, 2005.

[19] P.J. Pagni, T.P. Peterson, Flame spread through porous fuels, – in: Proceedings of the Fourteenth Symposium (International) on Combustion, The Combustion Institute, pp. 1099–1107. http://dx.doi.org/10.1016/S0082-0784(73)80099-2, 1973.

[20] W.J. Parker, Prediction of the heat release rate of douglas fir, – in: Proceedings of the Second International Symposium, International Association for Fire Safety Science, pp. 337–346. http://dx.doi.org/10.3801/IAFSS.FSS.2-337, 1989.

[21] T. Beer, I. Enting, Fire spread and percolation modelling, Math. Comput. Model. 13 (1990) 77–96. http://dx.doi.org/10.1016/0895-7177(90)90065-U.

[22] F.P. Incropera, D.P. De Witt, Fundamentals of Heat and Mass Transfer, John Wiley and Sons, New York, 1985.

[23] Y. Billaud, A. Kaiss, J.L. Consalvi, B. Porterie, Monte Carlo estimation of thermal radiation from wildland fires, Int. J. Therm. Sci. 50 (2011) 2–11. http://dx.doi.org/10.1016/j.ijthermalsci.2010.09.010.

[24] K. Kanatani, P. Rangarajan, Hyper least squares fitting of circles and ellipses, Comput. Stat. Data Anal. 55 (6) (2011) 2197–2208. http://dx.doi.org/10.1016/j.csda.2010.12.012.

[25] Z. Liu, H. Qiao, Multiple ellipses detection in noisy environments: a hierarchical approach, Pattern Recognit. 42 (11) (2009) 2421–2433. http://dx.doi.org/10.1016/j.patcog.2009.01.028.

[26] S.J. Ahn, W. Rauh, H.J. Warnecke, Least-squares orthogonal distances fitting of circle, sphere, ellipse, hyperbola, and parabola, Pattern Recognit. 34 (2001) 2283–2303. http://dx.doi.org/10.1016/S0031-3203(00)00152-7.

[27] Y. Qiao, S.H. Ong, Arc-based evaluation and detection of ellipses, Pattern Recognit. 40 (7) (2007) 1990–2003. http://dx.doi.org/10.1016/j.patcog.2006.10.009.

[28] J.C. Bezdek, J. Keller, R. Krisnapuram, N.R. Pal, Fuzzy Models and Algorithms for Pattern Recognition and Image Processing, Springer, New York, 2005. http://dx.doi.org/10.1007/b106267.

[29] J.S. Scire, F.R. Robe, M.E. Fernau, R.J. Yamartino, A User's Guide for the CALMET Meteorological Model (Version 5), Earth Tech Inc., Concord, MA, 2000 (Available at) ⟨http://www.src.com⟩.

[30] J. Silva, C. Ribeiro, R. Guedes, Roughness length classification of Corine LAND COVER classes, Proceedings of the European Wind Energy Conference, p. 110, 2007.

[31] P.H. Thomas, R.W. Pickard, Fire spread in forests and heathland materials, Report Forest Research, Her Majesty's Stationary Office, London, 1961.
[32] P.H. Thomas, The size of flames from natural fires, in: Proceedings of the Ninth Symposium (International) on Combustion, The Combustion Institute, pp. 844–859. http://dx.doi.org/10.1016/S0082-0784(63)80091-0, 1963.
[33] F. Nmira, J.L. Consalvi, P. Boulet, B. Porterie, Numerical study of wind effects on the characteristics of flames from non-propagating vegetation fires, Fire Saf. J. 45 (2010) 129–141. http://dx.doi.org/10.1016/j.firesaf.2009.12.004.
[34] G. Heskestad, Luminous heights of turbulent diffusion flames, Fire Saf. J. 5 (1983) 103–108. http://dx.doi.org/10.1016/0379-7112(83)90002-4.
[35] A.A. Putnam, A model study of wind-blown free-burning fires in: Proceedings of the Tenth Symposium (International) on Combustion, The Combustion Institute, 1965, pp. 1039–1046. http://dx.doi.org/10.1016/S0082-0784(65)80245-4.
[36] F.A. Albini, A model for the wind-blown flame from a line fire, Combust. Flame 43 (1981) 155–174. http://dx.doi.org/10.1016/0010-2180(81)90014-6.
[37] N.P. Cheney, J.S. Gould, W.R. Catchpole, The influence of fuel, weather and fire shape variables on fire spread in grasslands, Int. J. Wildland Fire 3 (1) (1993) 31–44. http://dx.doi.org/10.1071/WF9930031.
[38] N.P. Cheney, J.S. Gould, W.R. Catchpole, Prediction of fire spread in grasslands, Int. J. Wildland Fire 9 (1) (1998) 1–13. http://dx.doi.org/10.1071/WF9980001.
[39] P.A. Santoni, J.B. Filippi, J.H. Balbi, F. Bosseur, Wildland fire behaviour case studies and fuel models for landscape-scale fire modeling, J. Combust. (2011). http://dx.doi.org/10.1155/2011/613424.
[40] H.E. Anderson, Forest fuel ignitability, Fire Technol. 6 (1970) 312–319. http://dx.doi.org/10.1007/BF02588932.
[41] W. Mell, J.J. Charney, M.A. Jenkins, P. Cheney, J. Gould, Numerical simulations of grassland fire behavior from the LANL - FIRETEC and NIST - WFDS models, in: Proceedings. of the EastFIRE Conference, Fairfax, VA. http://dx.doi.org/10.1007/978-3-642-32530-4_15, 2005.
[42] W. Mell, M.A. Jenkins, J. Gould, P. Cheney, A physics-based approach to modelling grassland fires, Int. J. Wildland Fire 16 (2007) 1–22. http://dx.doi.org/10.1071/WF06002.
[43] A.L. Sullivan, Convective Froude number and Byram's energy criterion of Australian experimental grassland fires, in: Proceedings of the Thirty-First Symposium (International) on Combustion, The Combustion Institute, pp. 2557–2564. http://dx.doi.org/10.1016/j.proci.2006.07.053, 2007.
[44] U. Chaiyo, Y. Pizzo, S. Garivait, Estimation of carbon released from dry Dipterocarp forest fires in Thailand, Int. J. Environ. Ecol. Geol. Min. Eng. 7 (9) (2013) 609–612.
[45] M.C. Rochoux, B. Delmotte, B. Cuenot, S. Ricci, A. Trouvé, Regional-scale simulations of wildland fire spread informed by real-time flame front observations, in: Proceedings of the Thirty-Fourth Symposium (International) on Combustion, The Combustion Institute, 2013, pp. 2641–2647. http://dx.doi.org/10.1016/j.proci.2012.06.090, 2013.